Draft version January 2, 2019
Typeset using LaTeX **twocolumn** style in AASTeX61

THE GROWTH OF TWO DIMENSIONAL SUPERNOVAE IN CIRCULAR SECTORS

John M. Blondin[1] and Sena King[1]

[1] *Department of Physics, North Carolina State University, Raleigh, NC 27695-8202, USA*

ABSTRACT

Supernova explosions begin with the core collapse of massive stars, in which the spherical accretion shock instability (SASI) has been shown to play a key role. The origin of the SASI is under inquiry, and proposed mechanisms involve the radial and transverse propagation of the shock. Using the VH-1 hydrodynamics program, we are able to simulate the growth of supernovae in two dimensional circular sectors with arbitrary maximum angles. We attempt to isolate the transverse propagation of the shock by simulating two dimensional supernovae with fixed radii and varying sector angles. We then investigate the growth rate and angular speed of the SASI for simulations where we find isolated single arm ($m = 1$) spiral modes. We observe a nonlinear increase in the angular speed of the SASI as we reduce the sector angle, for small sectors below 1π radians. We observe linear, decreasing trends for the growth rate and angular speed of the SASI as we increase the sector angle, until the SASI begins to develop multiple spiral arms for large sector angles.

Keywords: accretion, accretion disks - hydrodynamics - shock waves - supernovae: general

1. INTRODUCTION

The contemporary model for supernovae involves a critical phase between the core-collapse of a massive star and the subsequent explosion, which is characterized by a stalled accretion shock. This phase can last on the order of a few hundreds of milliseconds (Mezzacappa 2005). Hydrodynamic simulations have demonstrated the existence of an instability in this stalled accretion shock, which has come to be known as the spherical accretion shock instability, or SASI (Blondin & Mezzacappa 2006).

The SASI has been demonstrated to grow into nonaxisymmetric "spiral" and "sloshing" modes as it evolves, even with no initial angular momentum (Blondin & Mezzacappa 2007). We will investigate the growth of these spiral modes in two-dimensional simulations, by analyzing the development of single arm $m = 1$ spiral modes.

The mechanism of the growth of the SASI is under inquiry, and the two dominant explanations are an acoustic mechanism and an advective-acoustic mechanism. The acoustic mechanism is dominated by transverse propagation, whereas the advective-acoustic cycle involves both transverse and radial propagation (Foglizzo et al. 2007). In a standard circle of inner angle 2π, the radius and circumference of a circle are related by a constant rate, so it is difficult to distinguish radial and transverse propagation by varying the radius of a supernova simulation.

In order to attempt to separate the radial and transverse propagation of the SASI, we will redefine the number of radians in a circle within the simulation model, so that it is possible to change the circumference of a two-dimensional supernova simulation without modifying its radius. In this paper, we seek to simulate supernovae using redefined maximum circular sector angles in order to distinguish between radial and transverse propagation of the SASI.

2. NUMERICAL MODEL

The simulation model presented in this paper is similar to previous two-dimensional supernova simulations (Blondin & Mezzacappa 2006; Blondin et al. 2017). We use the hydrodynamics code VH-1, modified to represent circular sectors with varying maximum angles. The boundaries $\theta = 0$ and $\theta = \theta_{max}$ are set to be periodic, so that matter can freely move across the bounds within the simulation. We use an ideal gas with an adiabatic index of $\gamma = 4/3$ on a disk with an outer radius of 2.0 subject to a Newtonian potentual $U = -GM/r$. We use the cooling parameters $\alpha = 3/2$ and $\beta = 5/2$ for a steady state accretion shock given by Houck & Chevalier (1992).

We use cooling rates set so that the steady state shock radius r_{sh} is equal to 1 for all simulations. We then evolve the supernova simulation in one dimension until the SASI begins to develop, and then export the data from the one-dimensional simulation to the two-dimensional simulations in order to reduce computation time.

We use 384 logarithmically placed grid zones in the radial direction for the one and two-dimensional simulations. For the grid count in the direction of θ, we divide θ_{sector} by the grid width in the radial direction, rounded to the nearest multiple of the number of processing cores. This ensures similar grid dimensions across all simulations.

For simulations with no initial specific angular momentum, the sector angle range where the SASI developed as a single $m = 1$ spiral mode was small and centered around 2π. To encourage the growth of spiral modes across multiple circular sector sizes, we initialize the two-dimensional simulations with specific angular momenta of 0.02 and 0.05, following the findings of Blondin et al. (2017) to enhance the growth of the SASI across a broader range of sector angles.

In order to visualize the growth of the SASI in circular sectors with maximum angles larger than 2π, we map the grid zones of the simulations to rectangular blocks. We also mapped the rectangular grid data into regular circular disks of size 2π, in order to compare the growth of the SASI across circular sector sizes.

We ran the simulations for circular sector values in the range of 0.1π to 10.0π, in steps of 0.1π.

We ran the simulations with inner radii r_* of 0.2, 0.4, and 0.55, with an initial angular momentum of 0.02. We also ran a simulation using $r_* = 0.2$ with an initial angular momentum of 0.05.

Given the results of Blondin et al. (2017), we expect that the simulations with a higher initial angular momentum will consistently have a greater angular speed. With the findings of Foglizzo et al. (2007), we expect that the simulation set with an inner radius of 0.55 will have a lower angular speed than the simulation set with an inner radius of 0.2.

3. ANALYSIS

We measure the strength of the SASI by computing the power in the $m = 1$ Fourier components of the deviation of angular momentum from the initial value, in a similar manner to Blondin et al. (2017). Using:

$$a(r) = \int_0^{2\pi} (h - rv_\phi) cos\phi d\phi \quad (1)$$

$$b(r) = \int_0^{2\pi} (h - rv_\phi) sin\phi d\phi \quad (2)$$

The amplitude of the SASI is derived from the radial integral of the full amplitude over the region of shocked gas,

$$C = \int_{r_*}^{r_s} \sqrt{a^2(r) + b^2(r)} dr \quad (3)$$

We extract the values w_r and w_i through least-squares fitting, where w_r corresponds to the angular speed of the SASI, and w_i corresponds to the growth rate of the SASI. To extract w_i, we take the logarithm of the amplitude of the growth curve and use linear regression over the linear segment as shown in Figure 1.To filter out noise, w_r is computed at a small region inside the shock boundary. The parameter w_r is contained in a periodic function given by $tan(w_r) = a/b$, so extracting it requires least-squares linear fitting across multiple periodic segments. We extract linear periodic segments with Pearson correlation coefficients of $r \geq 0.95$ and $r \leq -0.95$ (such that nonlinear segments are excluded) to calculate the angular speed of the SASI, as shown in Figure 2. By joining the extracted segments at π intervals, we can calculate a net wave speed over the segments. Both the scatterplot of the slopes of the periodic segments and the overall wave speed are shown below in Figure 3.

We note that the wave speed of the $m = 1$ modes of the SASI decreases in a convex pattern as the sector angle increases. The growth rate of the SASI, conversely, has a concave pattern that increases to a peak and then decreases. We observe that the angular speed of the SASI in Figure 4 is larger for simulations with an initial angular momentum of 0.05 as opposed the simulations with an initial angular momentum of 0.02, consistent with the findings of Blondin et al. (2017). We find that the angular speed of the SASI where the inner radius is 0.55 is greater than the angular speed of the 0.2 inner radius simulations. This is inconsistent with the findings of Foglizzo et al. (2007). The eigenfrequencies w_r and w_i are plotted using $|v_{sh}|/(r_{sh} - r_*)$ as the relative unit throughout the figures in this paper.

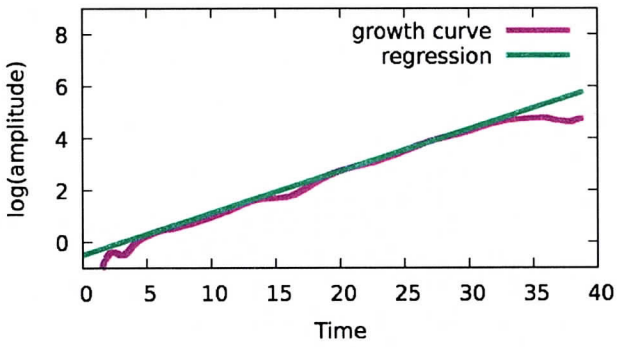

Figure 1. The growth curve for the circular sector $\theta_{sector} = 2\pi$, which we have extracted the growth rate from using least squares regression. The initial specific angular momentum for this specific growth curve is 0.02, and the inner radius of the core is 0.2. A regression of the growth curve for values of the natural logarithm of the amplitude from 0.05 to 3.0 is displayed as well.

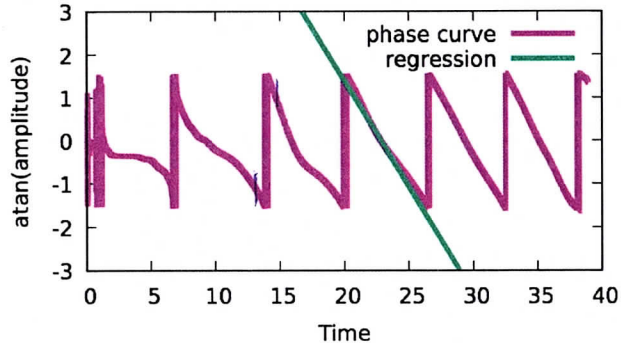

Figure 2. The phase curve for the circular sector $\theta_{sector} = 2\pi$, which we have extracted the angular speed from using least squares regression of the linear segments. The initial specific angular momentum is 0.02, and the inner radius of the core is 0.2. A regression of the linear segments of the arctangent of the phase curve is displayed as well.

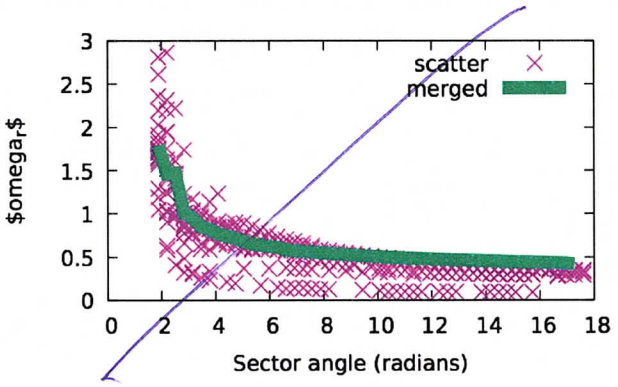

Figure 3. The angular speed of the SASI in simulations where the inner radius is 0.2 and the initial angular momentum is 0.02. A scatterplot of the slopes of the segments extracted from the phase curves is shown as well.

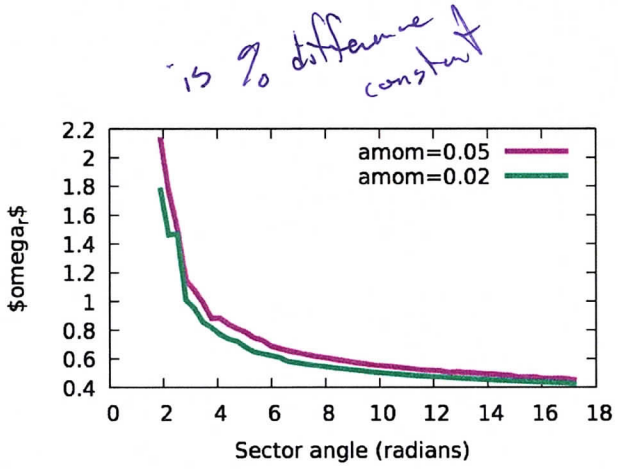

Figure 4. The angular speed of the SASI with $r_* = 0.2$, and different initial angular momenta.

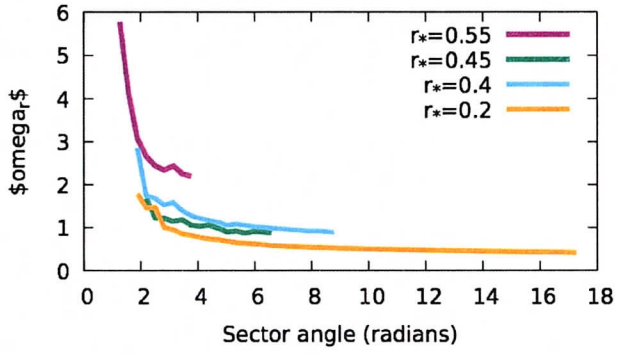

Figure 5. The angular speed of the SASI with an initial angular momentum of 0.02, and varying r_*.

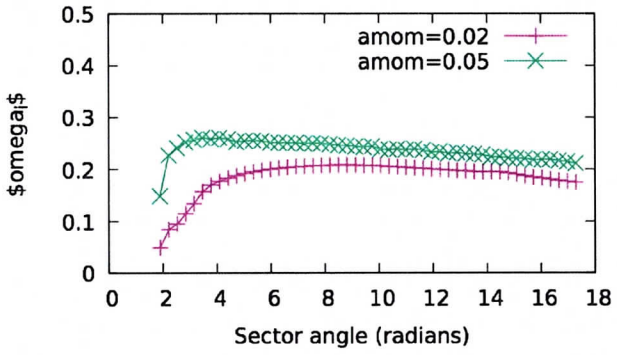

Figure 6. The growth rate of the SASI, with $r_* = 0.2$, and different initial angular momenta.

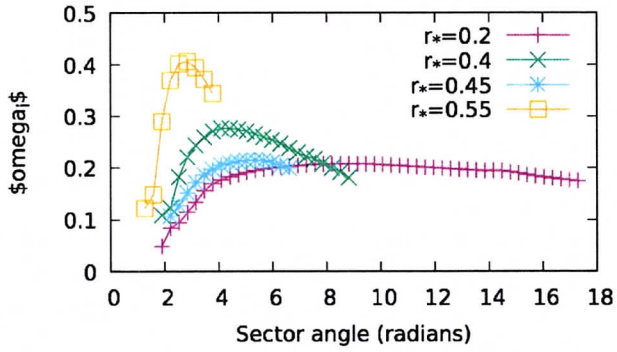

Figure 7. The growth rate of the SASI, with a fixed initial angular momentum of 0.02, and varying r_*.

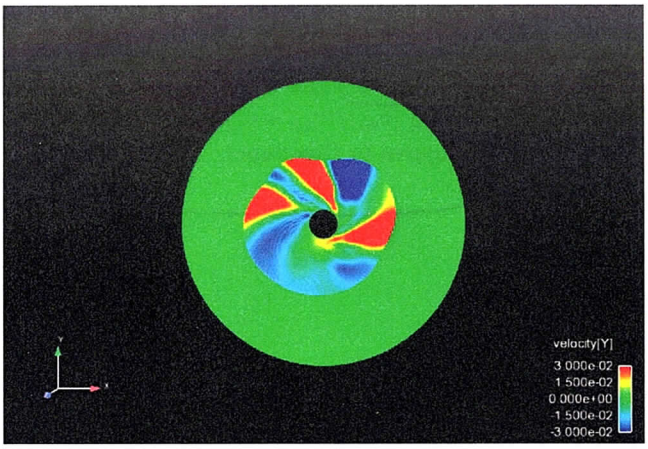

Figure 8. Circular sector with $\theta = 10\pi$, with an initial specific angular momentum 0.02 and inner radius 0.2, where multiple spiral modes appear ($m > 1$).

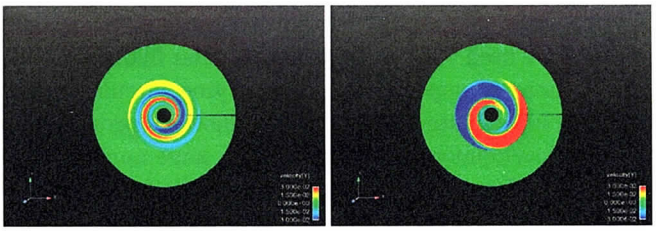

$\theta_{sector} = 0.6\pi$ $\theta_{sector} = 1.0\pi$

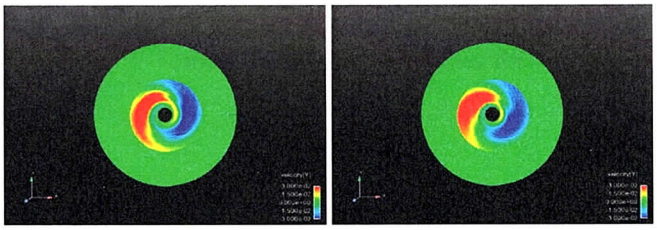

$\theta_{sector} = 2.0\pi$ $\theta_{sector} = 3.0\pi$

Figure 9. $m = 1$ spiral modes found in simulations with an initial specific angular momentum of 0.02 and inner radius 0.2, with their corresponding sector sizes. Figures are mapped to $\theta = 2\pi$ circles.

4. DISCUSSION

The dispersion relation in linear wave theory,

$$\omega = \sqrt{\frac{2\pi g}{\lambda} \tanh \frac{2\pi h}{\lambda}} \tag{4}$$

yields similar results to the angular speed of the $m = 1$ modes of the SASI plotted against sector angles.

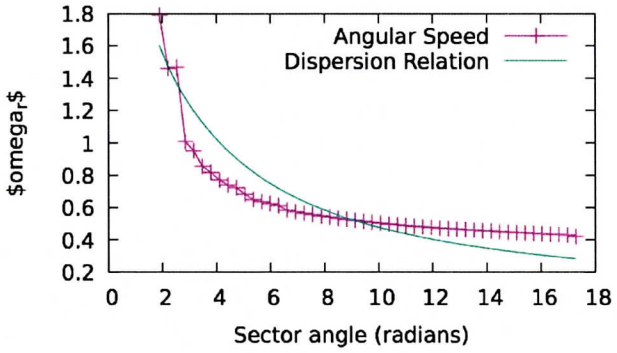

Figure 10. The angular speed of the SASI in simulations with $r_* = 0.2$ and an initial angular momentum of 0.02. The linear wave dispersion relation is shown as well.

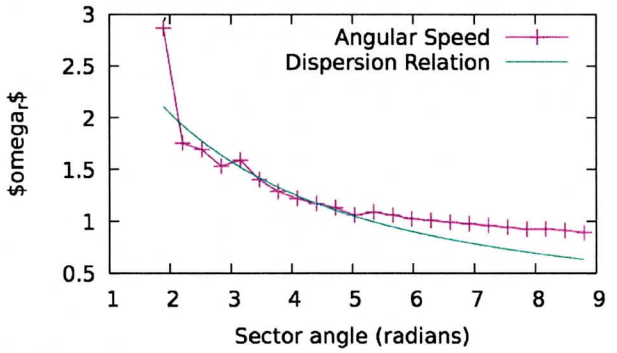

Figure 11. The angular speed of the SASI in simulations with $r_* = 0.4$ and an initial angular momentum of 0.02. The linear wave dispersion relation is shown as well.

Using 1.0 as the shock height, GM/r^2 as g (with $GM = 0.5$ and r as the shock height), and the sector angle as λ (as these are $m = 1$ modes) gives the dispersion relations as shown in Figure 10 and Figure 11. The linear wave theory equation 4 assumes a constant gravity with respect to radius in an incompressible fluid with no vorticity, none of which are applicable to the development of the SASI. However, the equation is capable of explaining the transition of the SASI from a deep depth to shallow depth context as the sector angle changes.

5. CONCLUSION

We have used two-dimensional, circular hydrodynamic simulations of supernovae with varying circular sector sizes to investigate the effects of transverse propagation in the development of the SASI. We have analyzed the growth and angular speed of $m = 1$ single arm spiral modes.

Our findings show that the angular speed of the SASI has a convex relation with respect to the sector angle, and that the growth rate of the SASI has a concave relation with respect to the sector angle.

REFERENCES

Blondin, J. M., Gipson, E., Harris, S., & Mezzacappa, A. 2017, ApJ, 835, 170

Blondin, J. M., & Mezzacappa, A. 2006, ApJ, 642, 401

Blondin, J. M., & Mezzacappa, A. 2007, Nature, 445, 58

Foglizzo, T., Galleti, P., Sheck, L., & Janka, H.-T. 2007, ApJ, 654, 1006

Houck, J. C., & Chevalier, R. A. 1992, ApJ, 395, 592

Mezzacappa, A. 2005, Annu. Rev. Nucl. Part. Sci., 55, 467

$$\omega = \sqrt{kg \tanh(hk)}$$

$$\omega = \frac{2\pi}{P} = \frac{2\pi C_s}{\lambda} = kC_s$$